Rev. Roum. Sci. Techn.– Électrotechn. et Énerg.
Vol. **68**, *4*, pp. 418–422, Bucarest, 2023

DEVELOPMENT OF METHANE CARBON ISOTOPE BASED ON MID-INFRARED ABSORPTION SPECTRUM TECHNOLOGY APPLIED IN LOGGING PLATFORM

CAIWEI FAN[1], YONGDE GAO[1], YITAO HU[2,4*], MAOLIN LIAO[2], JINBO WU[1], CHEN CHEN[3]

Keywords: Offshore drilling platform; Methane isotope; Mid-infrared tunable semiconductor absorption spectroscopy (TDLAS); Integral separated proportional-integral-derivative (PID) control method; High precision temperature control system.

To meet the requirements of rapid measurement of oil and gas methane isotopes in offshore logging platforms, a methane carbon isotope measurement system based on mid-infrared TDLAS technology was proposed in this paper. The measuring system adopted a mid-infrared compact-linear optical structure, including an interband cascade laser (central wavelength at 2 963.25 cm^{-1}), long optical path multi-pass cell (effective optical path is 24 m) and mercury cadmium telluride detector (response wavelength is from 2 μm to 5 μm). Combining two $^{13}CH_4/^{12}CH_4$ absorption lines, 2 963.25 cm^{-1} and 2 963.34 cm^{-1}, with a high precision temperature control system using an integral separation PID control method, a temperature fluctuation within 100 mK can be achieved. In the experiment, CH_4 gases with five different concentrations were configured to calibrate the measurement system, and the response linearity was more than 99%. When the integration time is 121s, the precision of isotope measurement was as low as 0.83 ‰. The average isotopic abundance of methane gas measured by the system was –10.2 ‰, and the error fluctuation was about ± 0.5 ‰. It was verified that the system can rapidly measure oil and gas methane isotopes.

1. INTRODUCTION

With the development of science and technology, human beings have gradually unveiled the mysterious veil of the ocean. The huge oil and gas resources in the deep sea make it the last resource treasury and strategic resource base of mankind. It has been found that there are a lot of oil and gas resources in the near seabed surface of the Sea South of China. If rationally exploited and applied, it will reduce the consumption of traditional fossil energy and alleviate the current energy crisis [1].

Logging technology is the "eye" of exploration and development. Methane carbon isotope detection technology is the key technology of logging. The first purpose of methane carbon isotope detection is to discover oil and gas layers directly. Second, the nature and genesis of oil and gas reservoirs can be analyzed. Third, it provides the data for further hydrocarbon accumulation and migration law studies. Therefore, it has become an urgent task to develop a rapid detection system of methane isotopes for oil and gas suitable for offshore drilling platforms [2,3].

At present, leading foreign research institutions have developed a variety of commercial instruments that can effectively obtain the methane isotope abundance of drilling platforms. Abroad, the real-time methane carbon isotope logging instrument developed by Geoservices, a Schlumberger subsidiary, solves the online isotope analysis problem [4]. However, the size of the equipment is large, and the influence of CO_2 and temperature changes on isotope data must be included. Many alkane (C1, C2, C3) isotope detectors have been developed in China, which can be analyzed online in small size. However, response times of several minutes still need to be increased to meet the rapid detection needs of offshore drilling platforms [5].

A methane carbon isotope detection system was developed independently considering the above status of offshore logging gas detection instruments and the actual project indicators based on mid-infrared TDLAS technology. Experiments show that the system can rapidly detect methane carbon isotopes.

2. THEORY OF ABSORPTION LINE SELECTION AND DETECTION

2.1. ABSORPTION LINE SELECTION

The principle of carbon isotope detection using TDLAS technology is the Beer-Lambert law, which is described as follows:

$$I(v) = I_0(v)e^{-\partial(v)CL}. \quad (1)$$

where I_0 is the initial intensity of the light source, $I(v)$ is the residual intensity after passing the measured gas, ∂(v) is the absorption coefficient of the measured gas, C is the concentration of the measured gas, and L is the effective absorption optical path length.

TDLAS technology is used to reduce the system $1/f$ noise and improve the performance of the detection system, where the second harmonic signal $2f$ is described as follows [6]:

$$I_{2f_{max}} = -k\partial_0 LCI_0(v), \quad (2)$$

where $I_{2f_{max}}$ is the peak value of the second harmonic signal $2f$, k is a constant that depends on the modulation depth, ∂_0 is the absorption coefficient at the central wavelength of the spectral absorption line.

The second harmonic component at the central frequency of the absorption line reaches its maximum value, which is proportional to the gas concentration. In this way, the concentration of $^{13}CH_4$ and $^{12}CH_4$ can be transformed into the following formula:

$$C = \frac{-k\partial_0 LI_0(v)}{I_{2f_{max}}}. \quad (3)$$

For CH_4 isotope abundance detection, $\delta^{13}C$ can be expressed as follows:

$$\delta^{13}\mathrm{C} = 1000 \times \left(\frac{[^{13}CO_2]/[^{12}CO_2]}{\mathrm{RPDB}} - 1\right)‰, \quad (4)$$

where RPDB is the international standard value of carbon isotope, and the value is 0.01124.

Since the absorption intensity of CH_4 carbon isotope line

[1] CNOOC China Limited-Zhanjiang, Zhanjiang 524057, China, E-mail: fancw@cnooc.com.cn, gaoyd1@cnooc.com.cn, wujb10@cnooc.com.cn
[2] Zhanjiang Branch of China-France Bohai Geological Service CO.LTD, Zhanjiang 524057, China, E-mail: huyt@cfbgc.com, liaoml@cfbgc.com
[3] College of Instrumentation & Electrical Engineering, Jilin University, Changchun 130026, China, E-mail: cchen@jlu.edu.cn
[4] School of Civil Engineering and Geomatics, Southwest Petroleum University, Chengdu 610500, China, huyt@cfbgc.com

DOI: 10.59277/RRST-EE.2023.68.4.16

contains temperature as a parameter. The temperature has different effects on the absorption intensity of CH_4 carbon isotope line. Therefore, the influence of temperature variation on isotope abundance detection results can be expressed as follows [7]:

$$\Delta\delta \approx \frac{\Delta T \cdot \Delta E}{k \cdot B \cdot T^2} \times 1000‰, \quad (5)$$

where $\Delta\delta$ is the variation of isotope abundance, ΔT is the fluctuation value of gas temperature, B is the Boltzmann constant, T is the absolute temperature constant, and ΔE is the energy difference between two pairs of absorption lines.

To reduce the influence of temperature fluctuations on CH_4 isotope detection. The absorption lines correspond to the smallest possible energy level difference. In addition, a highly stable temperature control system is required.

The high-resolution transmittance spectral line (HITRAN) database is a worldwide standard library for calculating and simulating atmospheric molecular transmission and radiation, covering a wide spectrum from microwave to ultraviolet light [8]. In the infrared band, the absorption spectrum is mainly composed of the vibration and rotation spectrum, and each gas has multiple absorption bands. Figure 1 depicts the HITRAN absorption spectra of CH_4 at a concentration of 100 ppmv at 40 Torr, 30℃, and an effective optical path length of 10.5 m.

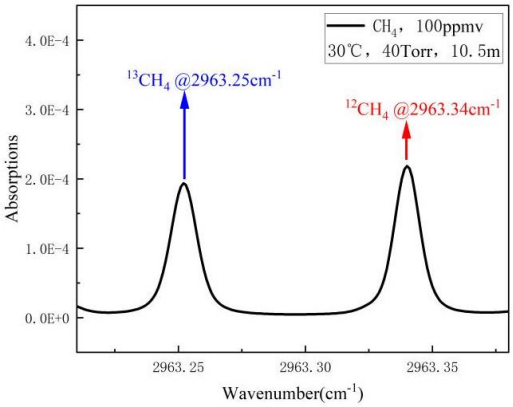

Fig. 1 – CH_4 isotope absorption spectrum.

The selection of CH_4 isotope absorption line pairs is very important for high-performance detection. The absorption line pairs of CH_4 isotopes are 2 963.25 cm^{-1} and 2 963.34 cm^{-1}, and the spectral spacing is narrow. Absorption line pairs do not overlap with H_2O, H_2S, and other chemical components. Furthermore, the absolute concentration of H_2O can be limited to less than 1% using a Nafion tube-based desiccator.

2.2. ABSORPTION LINE DETECTION

For CH_4 isotope detection, the intensity of the selected absorption line pairs provides a good signal-to-noise ratio for the detection system, which does not require a long gas absorption cell. Moreover, this improvement facilitates the miniaturization of the detection system. Because of the small energy difference between CH_4 carbon isotope absorption lines, the precision of isotope detection does not depend much on temperature. In particular, there are no water vapor absorption lines between pairs of carbon isotope absorption lines. Thus, the detection system needs to consider the influence of the ubiquitous water vapor [9].

The corresponding parameters of the selected CH_4 carbon isotope absorption spectral line pairs in eq. (5) are: $\Delta E = 4.76\times10^2$ cm^{-1}, $k = 1.9865\times10^{-23}$ J·cm, and temperature T is 300 K. For the detection target CH_4 isotope ratio of 1 ‰, the temperature change value should be less than 0.145 K. According to the empirical calculation of Allan variance, the precision of carbon isotope detection can be reduced to about 1 ‰, which meets the requirement of methane isotope detection of logging platform.

3. DETECTING SYSTEM CONFIGURATION

Figure 2 shows the methane carbon isotope logger, a linear structure with minimal physical size. The detection system is divided into two layers: the electrical system layer and the optical system layer.

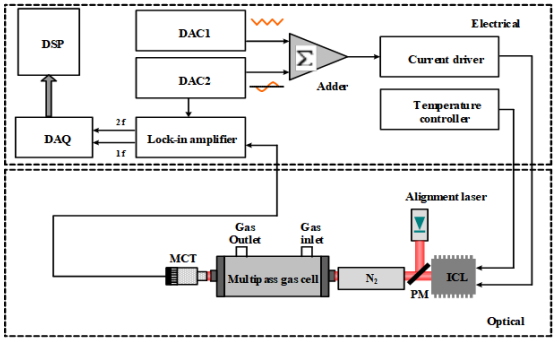

Fig. 2 – Structure diagram of methane isotope measuring system.

The optical system layer contains an interband cascade laser (Nanoplus GmbH), mercury cadmium telluride detector (Vigo, PVI-4TE-5), and self-developed long optical path multi-pass pool. A visible red He-Ne laser aligns the light path since the mid-infrared light source is free space light. The mid-infrared light passes through a pure nitrogen chamber into a long-path multipass cell, which is used to reduce interference from methane in the air. The long optical path multi-pass pool shell is made of stainless steel, and its thermal expansion coefficient is 10^{-6}/C. It provides an effective optical path of 10.5 m with a physical size of $20 \times 7.6 \times 10.5$ cm^3. The outgoing beam from the long path multi-pass cell directly enters the mid-infrared mercury cadmium telluride detector with thermoelectric refrigeration function (MCT).

The optical system layer contains an interband cascade laser (ICL) current driver and temperature controller, digital lock-in amplifier (Femto, LIA-MV-150), and digital signal processor (TI, TMS320F2812) as the electrical core components. ICL drive current and operating temperature device is the commercial current driver (Thorlabs, LDC202C) and temperature controller (Thorlabs, model TED200C). The triangular signal (0.5 Hz, 0.3 V) generated by the analog-to-digital converter DAC1, and the sine wave (5 kHz, 0.03 V) generated by the analog-to-digital converter DAC2 were loaded onto the current driver to scan and modulate the ICL wavelength. The analog-to-digital converter DAC2 provides synchronization signals to the digital lock-in amplifier (LIA) to ensure phase synchronization. Finally, the signal at the output of the LIA is passed through a data acquisition card (DAQ) and a digital signal processor (DSP) in the form of a second harmonic signal $2f$ related to isotope abundance.

An oil-free vacuum pump (Knf Neuberger, N813.5 ANE/AF) transfers gas samples into a long optical path multi-pass cell. Its pressure flow pressure controller (Bronkhorst, IQ+) control.

4. CHECK SYSTEM PERFORMANCE TESTS

4.1. ICL FUNCTIONAL TEST

The light source is ICL (physical size: 5 × 5 × 5 cm^3) in TO66 package manufactured by Nanoplus. The central wavelength of ICL is 3 374.67 nm (wave number is 2 963.25 cm^{-1}), the operating temperature is 39 ~ 43 ℃, and the operating current is 40 ~ 70 mA. A thermistor and a thermoelectric cooler are integrated inside the ICL chip, and the operating temperature is controlled by a temperature controller [10,11]. In addition, a collimating lens is placed in front of the ICL to align the emission beam. The emission spectrum of ICL was measured by Fourier infrared spectrometer (resolution 0.125 cm^{-1}), and the test results are shown in Fig. 3.

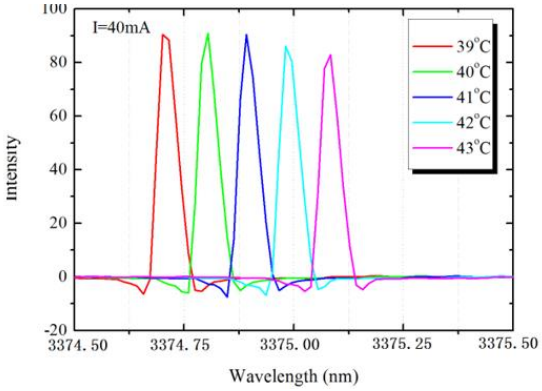

(a)

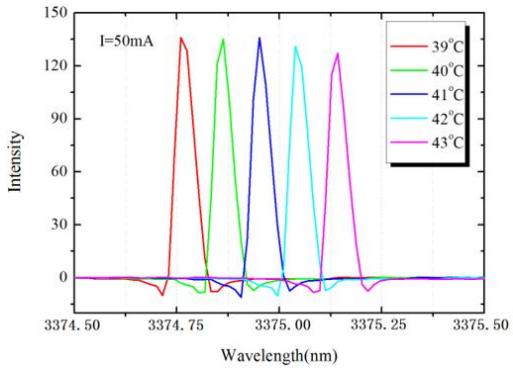

(b)

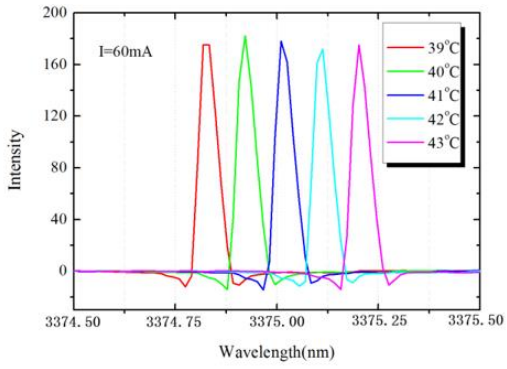

(c)

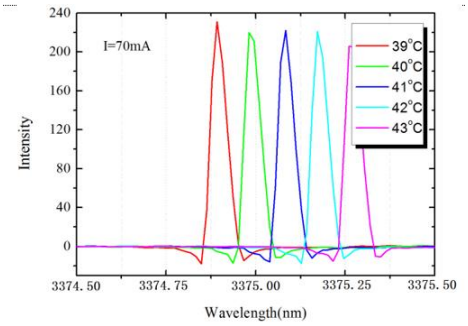

(d)

Fig. 3 – Output spectrum of ICL laser at different working temperatures when driving current is: a) 40 mA; b) 50 mA: c) 60 mA; d) 70 mA.

To control the ICL emission wavelength, the above spectrum is used to test the experimental data. The atlas of ICL emission wavelength, injection current, and operating temperature were established, as shown in Fig. 4.

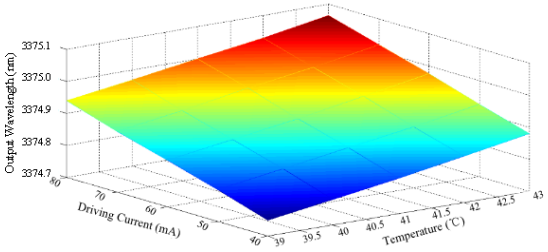

Fig. 4 – Spectrum map of ICL laser emitting wavelength.

When the ICL operating temperature is constant, its output center wavelength is linearly related to the operating current. With the ICL operating current constant, changing its operating temperature can effectively tune the ICL center wavelength. According to the experimental data, two important parameters of ICL are obtained: current tuning coefficient and temperature tuning coefficient. In the 40~70 mA temperature range of 39~43 °C, the current tuning coefficient is 0.06 nm/mA. The temperature tuning coefficient is 0.08 nm/°C.

4.2. CALIBRATION TEST OF DETECTION SYSTEM

Carbon isotopes can be accurately measured using a known gas concentration calibration system [12]. Five different concentrations of CH_4 of the above configuration were pumped into the long optical path multi-pass pool during the 5-minute measurement. The second harmonic signal peaks of $^{13}CH_4$ and $^{12}CH_4$ are shown in Fig. 5.

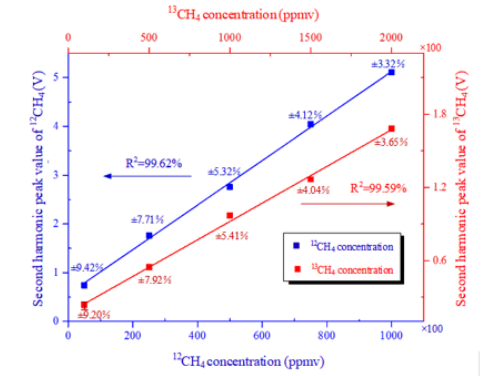

Fig. 5 – Concentration measurement results of 13CH4 and 12CH4 and their fitting curves.

Figure 5 shows the blue raw data representing the relationship between the average value of the second harmonic peak of $^{12}CH_4$ and the corresponding concentration. In addition, the raw data in red indicate the relationship between the mean value of the second harmonic peak of $^{13}CH_4$ and the corresponding concentration.

By linear fitting of the measured data, the following formula can be obtained:

$$^{13}CH_4 = 0.0000065 \times 2f(^{13}CH_4) + 0.35, \quad (6)$$

$$^{12}CH_4 = 0.000045 \times 2f(^{12}CH_4) + 0.6, \quad (7)$$

where $2f(^{13}CH_4)$ and $2f(^{12}CH_4)$ are the peak average values of the second harmonic signals corresponding to $2f(^{13}CH_4)$ and $2f(^{12}CH_4)$, respectively. The output response of the detection system is corrected by linear fitting, and the fitted formula inevitably introduces calibration deviation. For $^{12}CH_4$, the calibration deviation ranges ± 9.42 % to ± 3.32 %. The calibration deviation decreases with the increase of concentration. The calibration deviation of $^{13}CH_4$ ranges from ± 9.20 % to ± 3.65 %. The variation trend of calibration deviation is the same as that of $^{12}CH_4$. The above two formulas can be used to calculate the concentration of $^{13}CH_4$ and $^{12}CH_4$ by the peak value of the second harmonic signal. Therefore, the CH_4 isotope abundance value can be obtained.

4.3. DETECTION LIMIT TEST OF DETECTION SYSTEM

To assess the detection limit of the isotopic abundance of the system, the Allen variance was used for a concentration of 5 000 ppmv. Standard CH_4 with an isotope abundance of – 8.5 ‰ was measured for 60 minutes. The $2f$ signal was extracted, and the isotopic abundance $\delta^{13}C$ was calculated to obtain the Allen variance curve, as shown in Fig. 6.

As shown in Fig. 6a, the measured average value is – 10.2 ‰, and the fluctuation range is ± 0.5 ‰ (confidence interval is 80 %). The above experimental results show that the self-developed detection system has a good level of accuracy because the difference between the measured value and the standard value is only 1.7 ‰.

Considering that the measurement error of the detection system changes slowly, Allan variance is used to estimate the detection limit performance accurately. The results of the Allan variance analysis are shown in Fig. 6b, which shows the relationship between average time and Allan variance. The graph shows the relationship between average time and Allan variance.

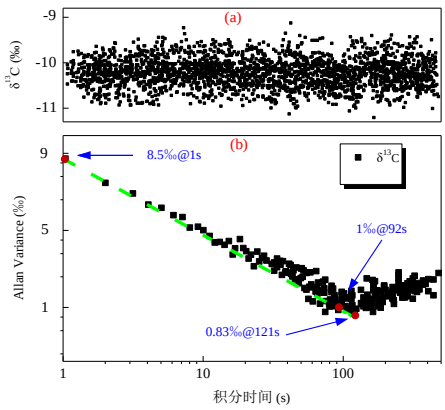

Fig. 6 – a) Long-term measurement results of isotope abundance; b) the relationship diagram of Allen variance and integration time.

As seen from Fig. 6, when the average time is 1, the detection limit is 8.5 ‰. As the average time increased to 92 s, the detection limit dropped to 1%. When the average time was 121 s, the detection limit decreased to 0.83 ‰. Since white noise is the main component before 121 s, the detection limit decreases with the increase of integration time. After 121 s, the detection limit starts to rise when drift becomes the dominant noise. The green dashed line represents the system response when white noise is the main noise of the system.

4.4. OIL AND GAS SAMPLE TESTING

The well W19 is deployed on the southern fault zone of Wenchang B Sag, and the main exploration strata are Zhuhai Formation and Enping Formation, and the buried hill of bedrock is also explored. The mature source rocks of the middle and deep lacustrine facies in the second member of the Wenchang Formation in the block where this well is located are of high quality and large thickness. A large inversion structure is developed on it, and the oil and gas formed by the middle-deep lacustrine source rocks can first migrate vertically through the gully source faults and their derived faults and then migrate laterally along the structural ridge to the trap through the transport and sand body. To further implement the characteristics of source rocks and hydrocarbon generation evolution of fluids in this block. After drilling, 55 single-point gas samples were returned to the base for measurement using the carbon isotope equipment developed in this paper. At the same time, verify the reliability and measurement accuracy of the equipment described in this paper. Using a gas chromatography analyzer, six gas samples were taken for synchronous measurement in the laboratory. The comparison between the measurement results and laboratory data of the equipment developed in this paper is shown in the following table. As can be seen from Table 1, the average absolute error between laboratory analysis and the measurement results of the proposed instrument is 1.2 ‰. Meanwhile, the measurements of methane carbon isotope at the same drilling site were carried out using the Grand3 instrument. The average absolute error between the drilling site analysis and the measurement results of this equipment is 0.78 ‰.

Table 1

Comparison of measurement accuracy of methane carbon isotopes

Well depth	Measurement results of this equipment	Laboratory data	Absolute error1	Field analysis	Absolute error2
(m)	(‰)	(‰)	(‰)	(‰)	(‰)
2073	-42.39	-43.98	1.59	-41.45	0.94
2103	-39.95	-39.01	0.94	-39.23	0.72
2113	-39.36	-40.47	1.11	-38.87	0.49
2123	-38.73	-39.66	0.93	-38.98	0.25
2135	-41.36	-40.39	0.97	-42.12	0.76
2146	-41.78	-40.28	1.50	-40.25	1.53

The measurement accuracy of methane carbon isotope equipment developed in this paper meets the technical specification of carbon isotope logging. The application effect is good, the equipment volume is small, the cycle is short, the cost is low, and it is more suitable for the field application. But at the same time, it also has a disadvantage that only carbon isotope parameters of methane can be measured, and the measured components are relatively single.

In addition, the 55 points measured by the equipment proposed in this paper belong to Section One of Enping Formation, and the methane carbon isotope values range from –42.39 ‰ to –39.0 1‰ [13,14], which are typical mature oil-type gas. Compared with the measured methane carbon isotope data of crude oil (condensate) in this structure, all the results have good consistency and belong to the same source fluid. Both come from the shore-shallow lacustrine source rocks of the Enping Formation. The supporting data are shown in Table 2.

Table 2

Methane carbon isotopes for multiple wells in the same stratum of the region

Well No.	Depth (m)	$\delta^{13}C$ (‰)
W9	3799.9	−43.73
	3860.6	−41.91
	3915.5	−39.44
	3954.5	−40.01
	3981.0	−41.13
W14	2877.3	−37.52
W19	2073.0	-42.39
	2103.0	-39.95
	2113.0	-39.36
	2123.0	-38.73
	2135.0	-41.36
	2146.0	-41.78

Real-time measurement of carbon isotopes can provide an essential basis for determining the origin and reservoir type of oil and gas and is of great significance for oil and gas exploration and development.

5. **CONCLUSION**

This paper presents a methane carbon isotope detection system based on mid-infrared TDLAS technology for offshore drilling platforms. Regarding absorption line selection, two $^{13}CH_4/^{12}CH_4$ absorption lines with low ground state energy level differences were used to pair 2 963.25 cm^{-1} and 2 963.34 cm^{-1}. In terms of optical composition, the system consists of ICL, MCT, and multi-pass cells with long optical paths to form a “compact-linear” optical structure. In the experimental test, the linearity of the system response can reach more than 99 %. When the integration time is 121 s, the precision of methane carbon isotope detection is as low as 0.83 ‰. The mean value of carbon isotope abundance was –10.2 ‰, and the error fluctuated about ± 0.5 ‰. Further work is needed to enhance the stability and reliability of the system to adapt to the complex offshore application scenarios and to explore the rapid measurement and analysis of carbon isotopes in more components.

Received on 13 March 2023

REFERENCES

1. J. Dai, *Significant of the study on carbon isotopes of alkane gases*, Natural Gas Industry, **31**, *12*, pp. 1–6 (2011)
2. D. Li, X. Guo, D. Wang, P.B. Ma et al. *Laser detection of oil-gas diffusion in central drain pipe of floating-roof tank*, Infrared and Laser Engineering, **42**, *5*, p. 913 (2021).
3. Z.Z. Wang, *Technical progress and developing trends in unconventional oil and gas mud logging in China*, Petroleum Drilling Techniques, **45**, *6*, pp. 1–7 (2017).
4. S.B. Hammerschmidt, T. Wiersberg, V.B. Heuer et al. *Real-time drilling mud gas monitoring for qualitative evaluation of hydrocarbon gas composition during deep sea drilling in the Nankai Trough Kumano basin*, Geochemical Transactions, **15**, pp. 1–15 (2014).
5. Q. Niu, Y.Y. Qu, X.H. Ci, W.Z. Zhou, H.X. Zhang, *Development status and prospect of carbon isotope logging technology*, Logging Engineering, **30**, *3*, pp. 8–15 (2019).
6. Q. Ren, C. Chen, Y. Wang et al. *A prototype of ppbv-level midinfrared CO_2 sensor for potential application in deep-Sea natural gas hydrate exploration*, IEEE Transactions on Instrumentation and Measurement, **69**, *9*, pp. 7200–7208 (2020).
7. S. Schaeffer, J. Miller, B. Vaughn *et al*. *Long-term field performance of a tunable diode laser absorption spectrometer for analysis of carbon isotopes of CO_2 in forest air*, Atmospheric Chemistry and Physics, 8, pp. 5263–5277 (2008).
8. L.S. Rothman, I.E. Gordon, Y. Babikov, *et al*. *The HITRAN 2012 molecular spectroscopic database*, Journal of Quantitative Spectroscopy & Radiative Transfer, **130**, pp. 4–50 (2013).
9. K. Jian, S.X. Liu, Y.L. Chen, X.H. Fu, *Infrared spectroscopic study on the structure evolution of low-rank coal and its correlation with carbon isotope of alkane gas in pyrolysis process*, Spectroscopy and Spectral Analysis, **38**, *7*, pp. 2070 (2018).
10. M.L. Cong, L. Li, Y.S. Cui, Z.Q. Zhang, Y.D. Wang, *Design of high stability digital control driving system for semiconductor laser*, Optics and Precision Engineering, **18**, *7*, pp. 1629–1636 (2010).
11. K.J. Åström, T. Hägglund, *Revisiting the Ziegler–Nichols step response method for PID control*, Journal of Process Control, **14**, 635–650 (2004).
12. C. Chen, W.N. Robert, Y.D Wang, *A trace methane gas sensor using mid-infrared quantum cascaded laser at 7.5 μm*, Applied Physics B: Lasers and Optics, **113**, *4*, pp. 491–501 (2013).
13. B.W. Wang, X.D. Xu, Y.U. Wu, *Oil-gas origin and accumulation characteristics of Wenchang Depression, Western Pearl River Mouth Basin*, Natural Gas Geoscience, **31**, *7*, pp. 980–992 (2020).
14. Y.Z. Zhang, X.D. Xu, L. You, *Genesis of the natural gas in tight condensate gas reservoirs and forming model, Wenchang a sag of Pearl River Mouth Basin*, Natural Gas Geoscience, **25**, *9*, pp. 1320–1328 (2014).